

Performance Characteristic of Two Color Midwave HgCdTe Detectors Above 80K

August 1998

Whitney Mason* and J. R. Waterman
Naval Research Laboratory
Washington, D.C. 20375

ABSTRACT

Two color mid-wave triple layer heterojunction HgCdTe detectors were studied using temperature-dependent current-voltage ($I - V$) measurements, temperature-dependent spectral response measurements, and temperature-dependent noise measurements. The reverse biased dark current shows diffusion-limited behavior for $T > 125K$. The same data shows evidence for generation-recombination type behavior at temperatures between 100K and 125K. For temperatures less than 100K, the measurements are limited background by photon flux, even though these measurements are performed at nominal zero background. The upper junction shows reverse breakdown voltages on the order of about 400mV, while the bottom junction shows no breakdown for $V < 500mV$. At 80K, the R_0A product is in excess of $1 \times 10^6 \Omega - cm^2$. In forward bias, the current-voltage characteristics of the lower junction are diffusion limited for all temperatures, while at lower temperatures, the upper junction showed generation-recombination behavior. Optical measurements found a cutoff wavelength of about 4 μm for the lower junction and about 4.5 μm for the upper junction. The temperature dependence of the cutoff wavelength agrees with theory. The spectral crosstalk was less than 5%. At 80K, the noise of the shorter wavelength junction could not be distinguished from the instrument noise, regardless of bias. For the longer wavelength junction, the noise at lower frequencies increases with bias. There is no difference in the noise characteristics when either the photon flux or the temperature is increased.

1.0 INTRODUCTION

Two-color midwave HgCdTe heterojunction based infrared focal plane arrays (IRFPAs) are being developed for tactical aircraft missile approach warning sensors. These sensors operate in high ambient temperature environments on the aircraft, $\sim 70^\circ C$, making sensor power dissipation a critical issue. Total sensor power is dominated by the focal plane cooler, so that the ability to operate at temperatures above the 90K currently employed using InSb focal planes, offers significant opportunity for sensor power reduction. To this end, we have investigated the performance of such detector test structures in the temperature range from 80K to 180K. Here we report on temperature dependent current-voltage ($I - V$) measurements, temperature-dependent spectral response measurements, and noise measurements, both as a function of temperature and bias.

2.0 DETECTOR

Santa Barbara Research Center has fabricated 128×128 focal plane arrays for use in two-color MWIR applications¹. These FPAs consist of stacked $n - p - n$ triple layer heterojunction (TLHJ) devices in HgCdTe grown by MBE on CdZnTe substrates, as shown in figure 1. These detectors consist of two back to back $p - n$ heterojunctions. The bandgaps are determined by the alloy composition of the $Hg_{1-x}Cd_xTe$ with a nominal value of $x \approx 0.335$ in the MWIR-1 layer, $x \approx 0.36$ in the p -type layer, and $x \approx 0.32$ in the MWIR-2 layer. The net donor concentration in both n -type layers is $N_D \approx 3 \times 10^{15} cm^{-3}$, while the net acceptor concentration in the p -type layer is $N_A \approx 1 \times 10^{18} cm^{-3}$. The layer thicknesses are chosen to provide a sharp cutoff wavelength; the corresponding widths are: MWIR-1 $10\mu m$, the cap layer about $5.5\mu m$, and the MWIR-2 layer about $6\mu m$. The detectors are back-illuminated through the substrate. The shorter wavelength photons are absorbed by the lower n -type (MWIR-1) layer and captured at the lower $p - n$ junction. This layer also acts as a filter, only allowing longer wavelength photons to pass into the MWIR-2 layer. These diodes were produced in both a single and double mesa format with junction areas of approximately $2 \times 10^{-5} cm^2$.

Figure 2 shows a unit cell for both single and double mesa architectures. The double mesa architecture is the established method for two-color applications; it provides for greater than 65% fill factor in the MWIR-2 layer. The novel single mesa architecture provides for greater than 80% fill factor in the MWIR-2 layer. (Both architectures provide 100% fill factor for the MWIR-1 layer.)

3.0 I-V MEASUREMENTS

$I - V$ characteristics were measured as a function of temperature for both single- and double-mesa architectures. These were also measured as a function of position in the array: the center of the array, the interior of the array (but not at the center), and the perimeter of the array. Figure 3 shows typical $I - V$ curves at $80K$ at nominal zero background for the longer cutoff wavelength top junction, and shorter cutoff wavelength bottom junction, located at the edge of the array. At a reverse bias of about $50mV$, dark current densities of $10nA / cm^2$ and $90nA / cm^2$ were observed for the upper and lower junctions respectively. Both junctions exhibit open circuit voltages of about $50mV$. Therefore, a significant fraction of this "dark current" is attributed to photocurrent resulting from non-optimal cold shielding. The photocurrents are equivalent to photon fluxes of only 5×10^{10} and $5 \times 10^{11} photons / sec \cdot cm^2$. The temperature dependence of this zero bias R_0A is shown in figure 4. At $80K$ the R_0A product calculated from the reverse biased dark current is on the order of $1 \times 10^6 \Omega - cm^2$, and remains greater than $10^4 \Omega - cm^2$, consistent with background limited performance for the missile warning application, up to $146K$. The activation energy derived from a curve of this R_0A versus the inverse temperature is systematically larger than the cutoff wavelength found from spectral response measurements with a scatter about the average as large as 10% due to complications from excess photocurrent at reverse bias. This increase may be attributed to generation from the cap layer. Therefore, R_0A was calculated from the forward bias $I - V$ characteristics at biases such that the current greatly exceeds the photocurrent. Figure 5 shows this R_0A as a function of inverse temperature for both junctions shown in figure 3. The activation energy of $0.288eV / K$ for the top junction indicates diffusion-limited behavior for $T > 130K$. For temperatures less than about $130K$, there is evidence of generation-recombination for the top junction. This is shown in figure 5 with an energy of $0.144eV / K$, which is exactly half the energy at higher temperatures. This behavior was not seen for the lower junction.

¹ J.E. Jensen, R.D. Rajavel, O.K. Wu, and D.M. Jamba, *Proc. of the 1997 Mtg. of the IRIS Specialty Group on Infrared Detectors*, p. 361. (1998).

The behavior shown here is typical of all the longer wavelength junctions tested. For the shorter wavelength junction, a plot of $R_0 A$ as a function of inverse temperature indicates diffusion limited behavior (for forward bias) for all temperatures. The activation energies ranged from $284 - 322 \text{ meV}$ for the lower junction and from $258 - 291 \text{ meV}$ for the upper junction. The upper junction shows reverse breakdown voltages ($I > 10^{-10} \text{ amps}$) of approximately 400 mV , while the bottom junction shows no breakdown for voltages less than 500 mV .

Unfortunately, it was difficult to perform any statistical analysis on the uniformity of the activation energies derived from this method, and therefore difficult to make any quantitative statement about the performance of the diodes based upon the architecture and placement in the array because only thirty-two of the devices were wired and not all of these met the required specifications. However, no real difference could be distinguished between the two types of device architecture, which is promising. This suggests that there is no degradation of performance when the single-mesa architecture is used, and it is more beneficial due to the above mentioned filling factor considerations. In addition, there is no clear trend of behavior based upon the placement of the device in the array.

4.0 SPECTRAL RESPONSE MEASUREMENTS

Spectral response measurements taken at 80 K under flood illumination, shown in figure 6, found a cutoff wavelength of $3.92 \mu\text{m}$ for the lower junction and $4.49 \mu\text{m}$ for the upper junction, with spectral crosstalk away from the cross-over region less than 5% . The intensity of the response for the shorter wavelength junction increased with increasing temperature, finally coming to some equilibrium value at higher temperatures, while the response for the longer wavelength junction remained essentially constant, as shown in figure 8. In order to ensure that this temperature dependence was not due to anomalous lateral collection from some region away from the junction, focused spot broadband blackbody measurements were performed. This data exhibits the same temperature dependence as the wavelength dependent measurement. This fact leads us to believe that the temperature-dependent intensity is real. In addition, there is a shoulder on the long wavelength side of the shorter wavelength spectral response that increases with temperature, shown in both figures 7 and 8. This corresponds to increased spectral crosstalk for long wavelength response in the shorter wavelength junction. The mechanism for this shoulder is not currently understood.

The value of the optical energy gap of $\text{Hg}_{1-x}\text{Cd}_x\text{Te}$ follows the Schmidt-Hansen-Casselmann equation², given by

$$E_g = -0.313 + 1.787x + 0.444x^2 - 1.237x^3 + 0.932x^4 + (0.667 - 1.714x + 0.760x^2) \frac{T}{1000}$$

for $T > 70 \text{ K}$, where E_g is given in eV , T is in K , and x is fraction of CdTe . Figure 9 shows a comparison of the cutoff wavelength found with the above equation. For the longer wavelength junction, the equation fit quite nicely to the data using $x = 0.3125$, which is close to the expected value of $x \approx 0.32$. For the shorter wavelength junction, the equation fit to the data using $x = 0.336$, which is very nearly the exact number expected. The data fits well to this equation at lower temperatures; however, at $T \approx 120$, the data begins to deviate from the expected values, being *larger* than the equation suggests. If we ignore the existence of the anomalous shoulder in the spectrum and extrapolate between the data points, we find the curve given in the bottom trace of figure 9, which agrees very well.

² G.L. Hansen, J.L. Schmidt, and T.N. Casselman, *J. Appl. Phys.* **53**, 7099 (1982).

5.0 NOISE MEASUREMENTS

At $80K$, an examination of the noise characteristics of the shorter wavelength junction was inconclusive, as the detector noise was less than the instrumentation noise floor (approximately equal to $0.1pA / \sqrt{Hz}$) for all biases less than or equal to $600mV$. The same result was found for the longer wavelength junction for all biases less than $100mV$. However, for reverse biases greater than or equal to $100mV$, the noise current is both frequency-dependent for frequencies less than about $1000Hz$, following a f^{-5} dependence, and bias-dependent, getting larger as the reverse bias gets larger. The current noise changes by about two orders of magnitude from a bias of $50mV$ to $600mV$. At $50mV$, with a dark current density of $7.5nA / cm^2$, the current noise at $1Hz$ is $5.04pA / \sqrt{Hz}$. At a reverse bias of $600mV$, with a dark current density of $1.85 \times 10^{-1} \mu A / cm^2$, the noise current at $1Hz$ is $5.38 \times 10^{-2} pA / \sqrt{Hz}$. Theoretical calculations³ found that the frequency-dependent noise current will follow the form

$$I_{noise} = \alpha \frac{I_t^\beta}{f^\delta}$$

where I_{noise} is given in A / \sqrt{Hz} , I_t is the tunneling current, α is a constant, $\beta \approx 1/2$, and $\delta \approx 1/2$. Figure 10 shows current noise as a function of frequency for a reverse bias of $200mV$, which is typical of all other biases greater than $100mV$. We found that $0.38 < \delta \leq 0.5$, for the different biases, increasing as the bias is decreased. Figure 11 shows the noise current as a function of the tunneling current with $\beta = 1/2$. The slope is $\alpha = 3.83 \times 10^{-4}$, which is two orders magnitude larger than that found in reference 3. When the temperature is increased up to $180K$, or the devices are exposed to radiation up to a factor of five over the $295K$ background radiation, there is no change in the noise characteristics, further suggesting that the noise is not diffusion current or generation-recombination related.

6.0 CONCLUSIONS

Two-color midwave HgCdTe detector test structures were studied extensively. The R_0A product calculated from both forward- and reverse-biased $I - V$ characteristics indicate diffusion-limited behavior for both junctions down to $T \approx 130K$. The upper junction shows generation-recombination behavior for $T < 130K$ with an activation energy half that of the diffusion-limited temperatures. No systematic differences were observed between the two different mesa architectures, nor could any differences be attributed to the placement of the diode in the array. Spectral response measurements showed a cutoff wavelength of about $4.5\mu m$ for the upper junction and about $4.0\mu m$ for the lower junction. Spectral crosstalk at $80K$ was less than 5%, with the spectral crosstalk of the upper junction increasing as the temperature increases. The noise measurements suggest that the noise in the frequency-dependent regime is limited by tunneling current, as the noise characteristics are neither temperature- nor radiation-dependent.

The occurrence of generation-recombination currents, soft tunnel breakdown, and excess low frequency noise for the top junction implies that the electrical quality of the top junction is inferior to that of the bottom junction. This may be attributed to difficulty in obtaining high quality base layer growth on

³ Y. Nemirovsky and A. Unikovsky, J. Vac. Technol. B **10**, 1602 (1992).

top of the As-doped cap layer. In spite of this, the performance of these devices is adequate for missile warning applications for operating temperatures up to $146K$. Further improvements in the junction quality would allow for BLIP operation under reduced flux conditions.

This work was supported by the Office of Naval Research.

- ASEE Post-doctoral fellow.

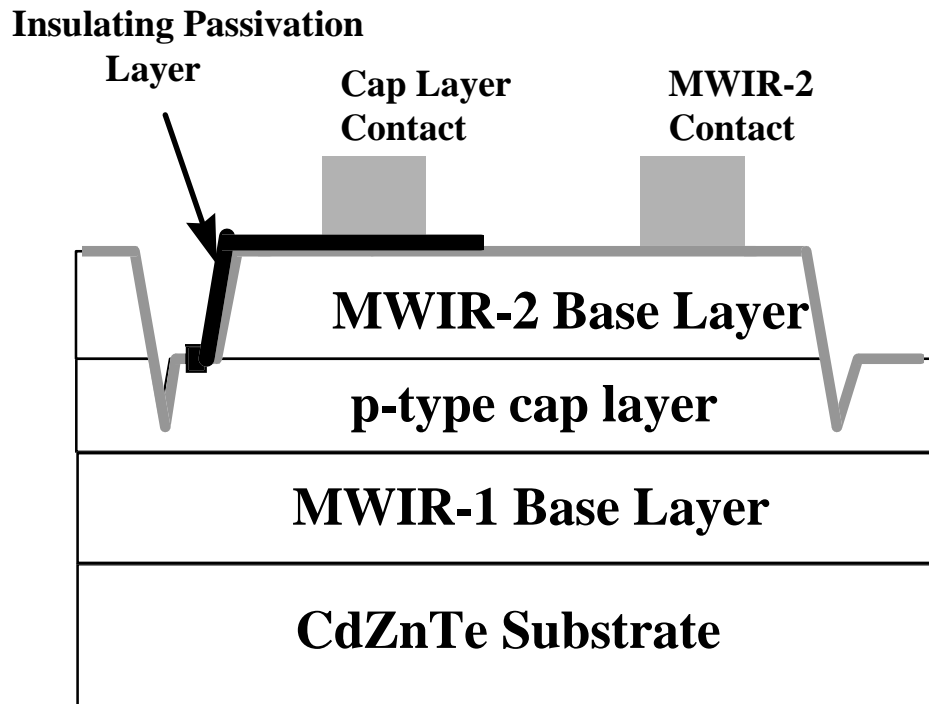
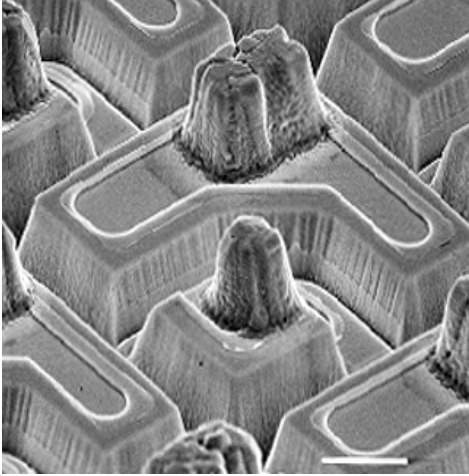


Figure 1. Schematic picture of the TLHJ. Mid-1 Base Layer is the array common, and also where the shorter wavelength photons are captured. Mid-2 Base Layer is where the longer wavelength photons are captured.

DOUBLE MESA



SINGLE MESA

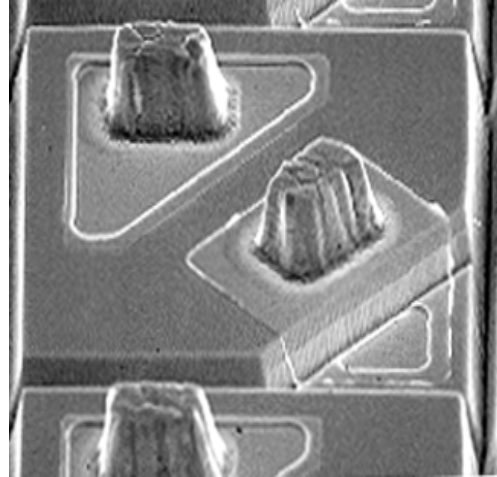


Figure 2. Unit cell layout for the two-color simultaneous detector discussed here. The double mesa structure on the left is the traditional architecture for these devices; it provides $> 65\%$ fill factor in the MWIR-2 layer. The single mesa architecture on the right provides $> 65\%$ fill factor in the MWIR-2 layer.

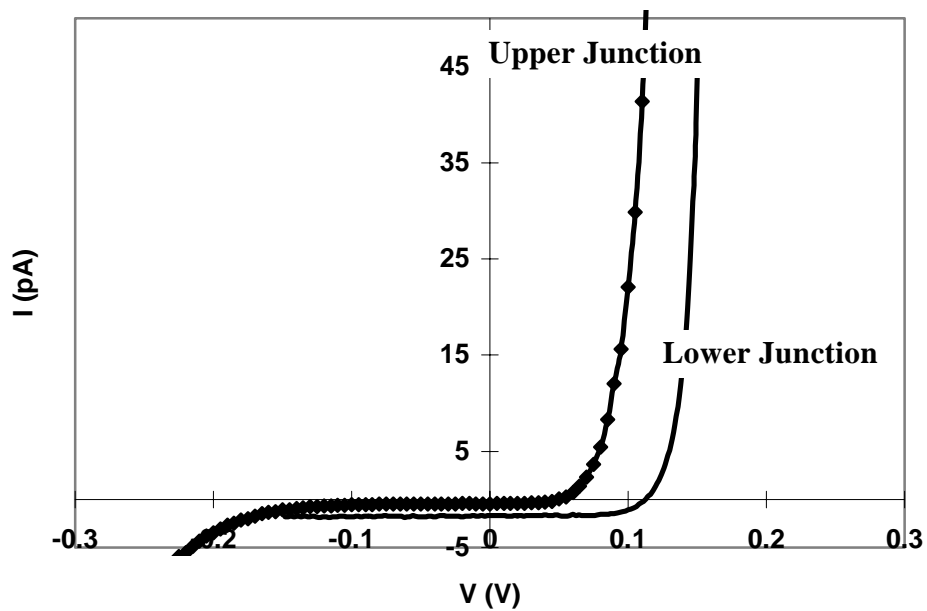


Figure 3. $I - V$ curves at nominal zero background for a single-mesa upper and lower junction located at the edge of the array.

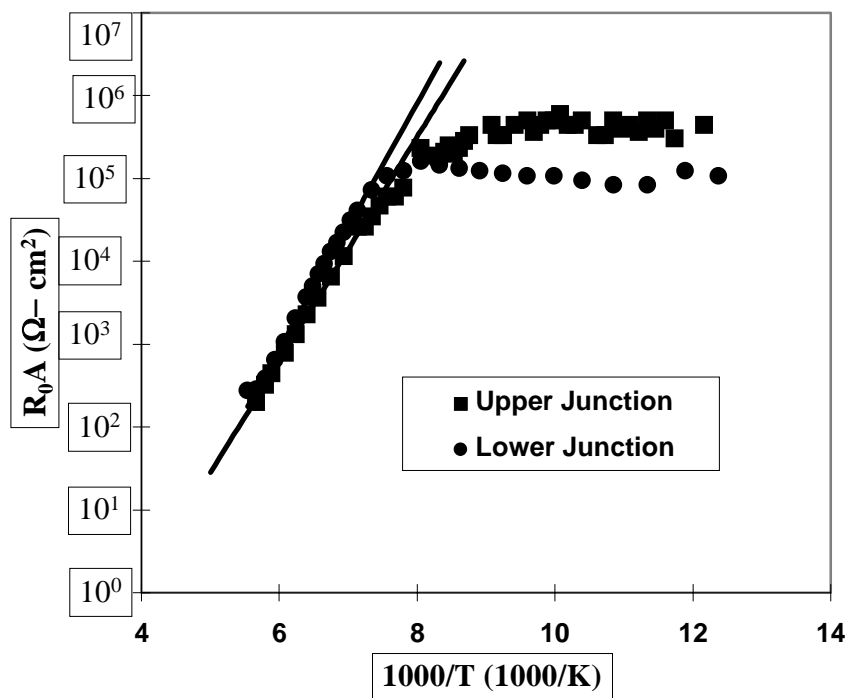


Figure 4. R_0A from reverse bias dark current as a function of inverse temperature for both junctions shown in figure 3.

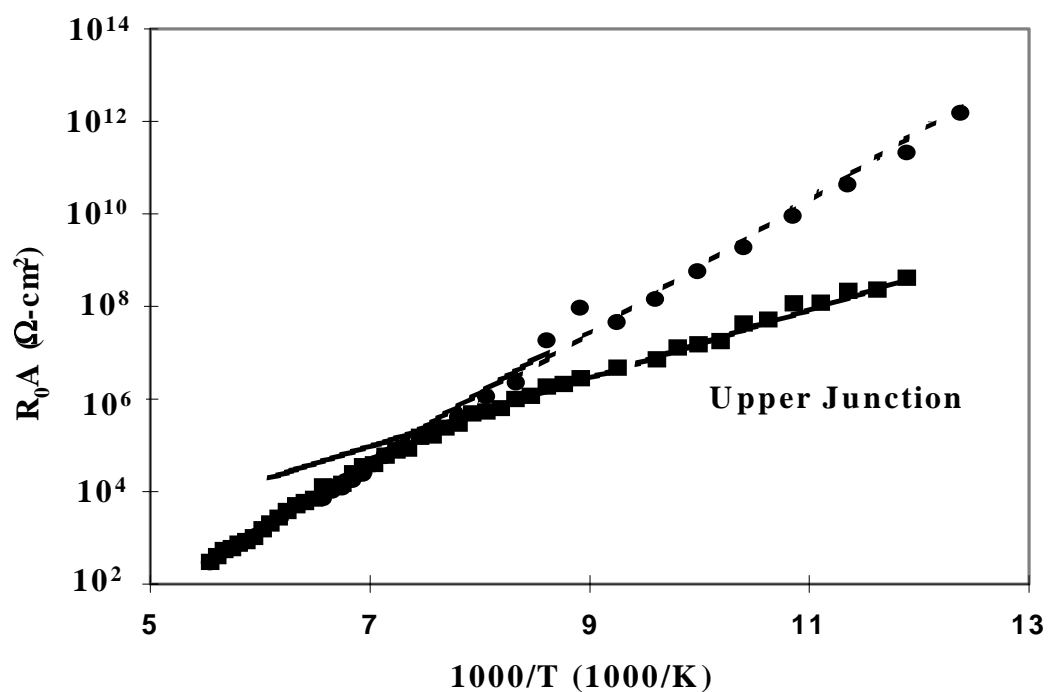


Figure 5. R_0A calculated from forward bias characteristics as a function of inverse temperature for both junctions shown in figure 3.

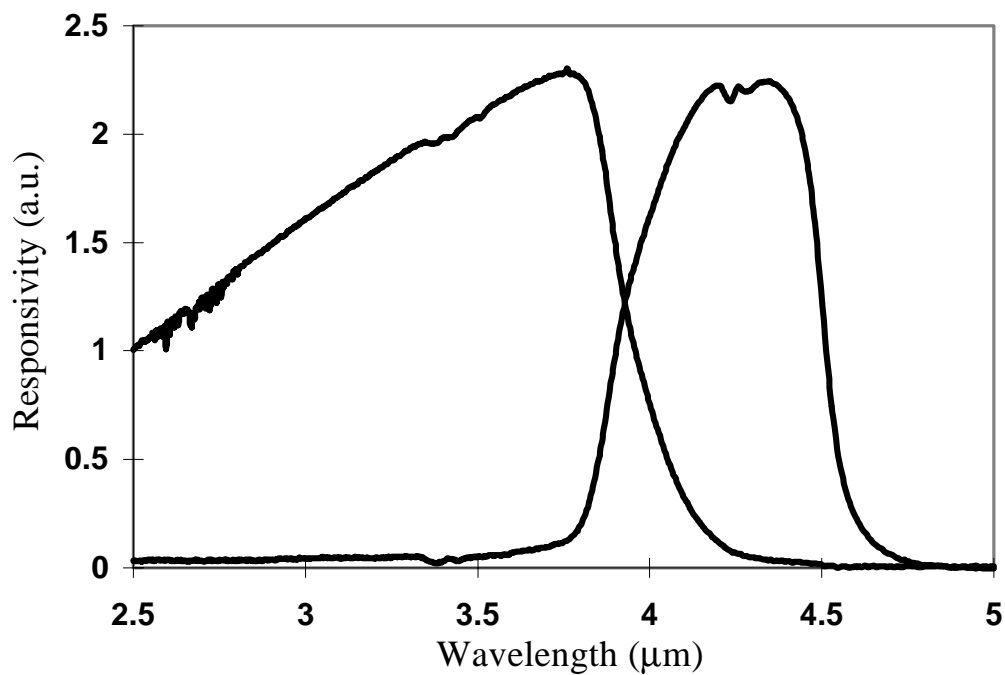


Figure 6. Relative responsivity for both junctions for a single-mesa architecture, centered device. The shorter wavelength junction has a cutoff wavelength of about $3.92\mu m$ and the longer wavelength junction has a cutoff of about $4.49\mu m$.

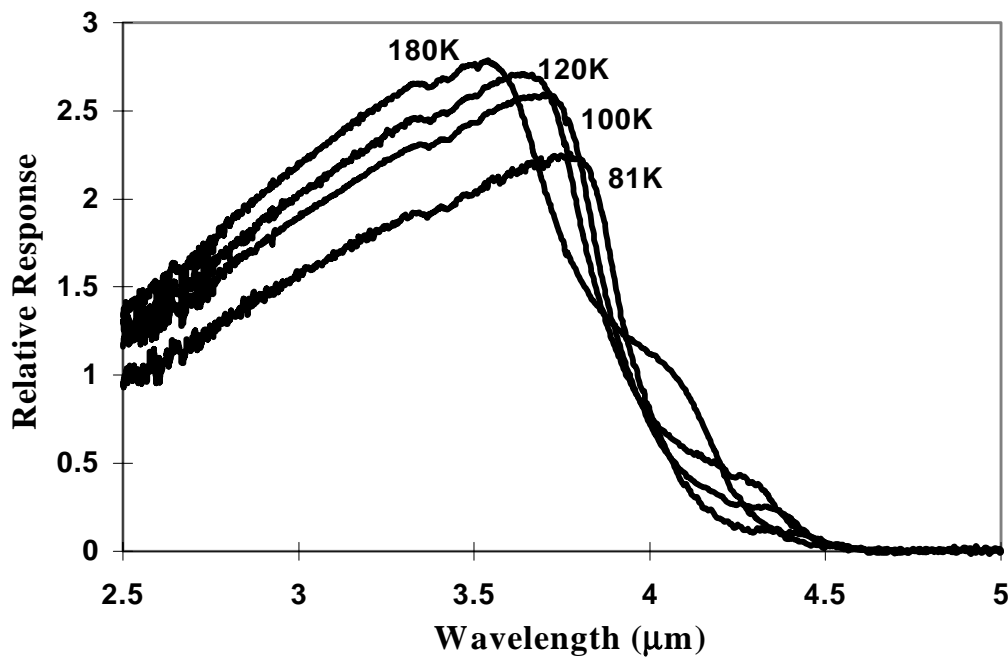


Figure 7. Relative response as a function of wavelength for the shorter wavelength junction for some representative temperatures. Notice how there is an anomalous longer wavelength response that appears as the temperature is increased.

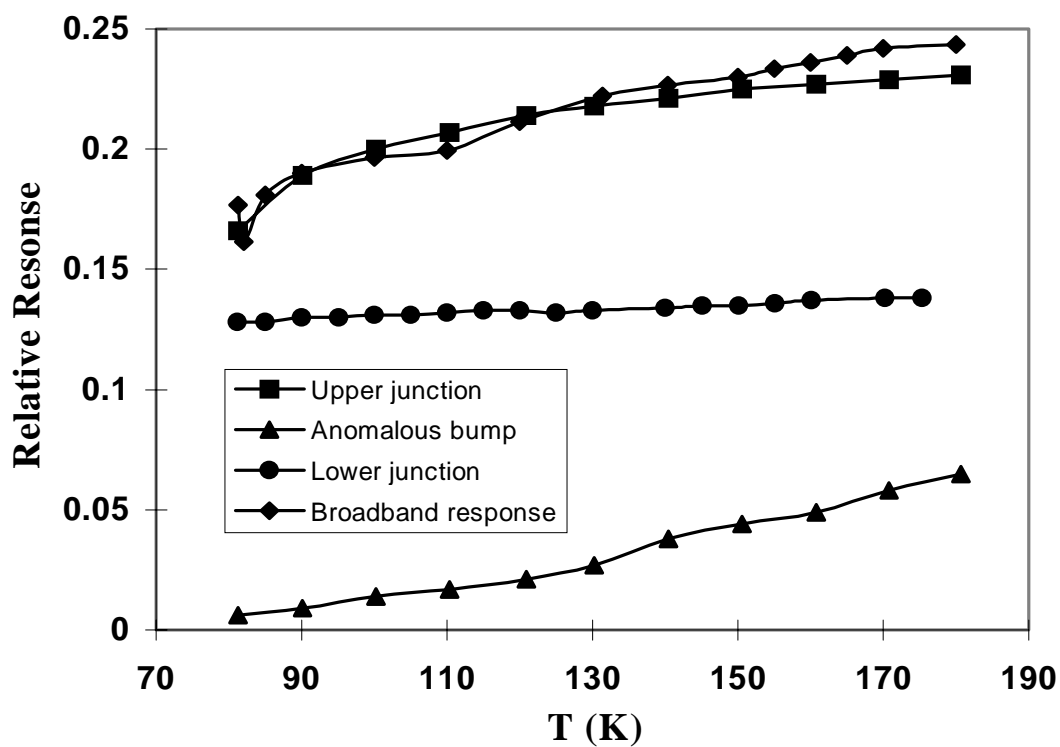


Figure 8. Intensity of the spectral response measurements as a function of temperature. The upper three data sets are for flood illumination; the bottom trace is for focused spot measurements.

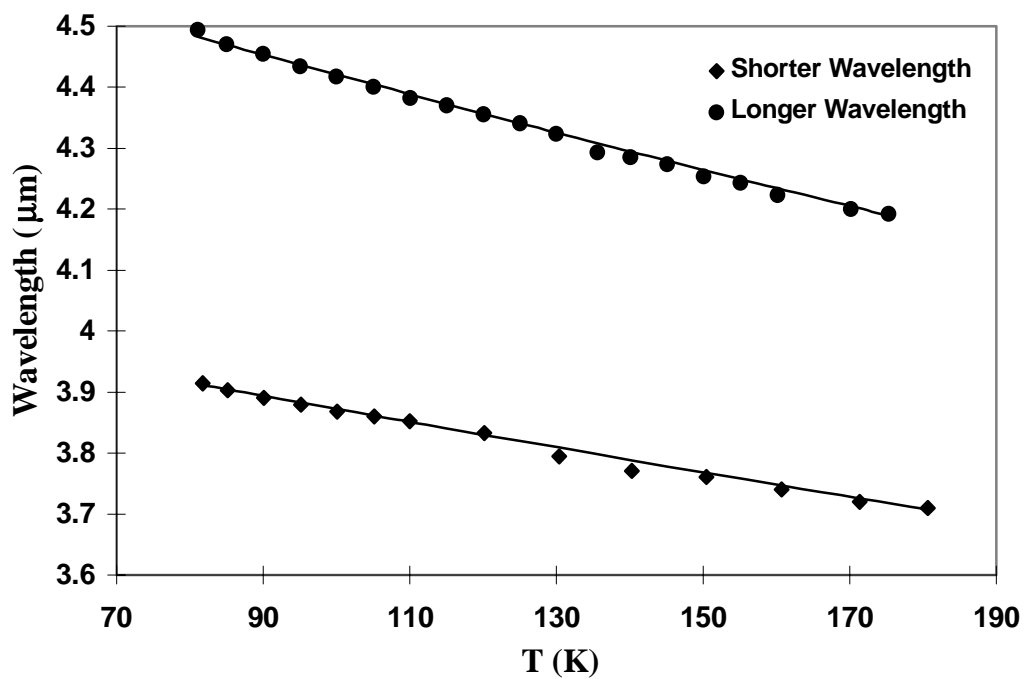


Figure 9. Temperature-dependence of the cutoff wavelength for both junctions.

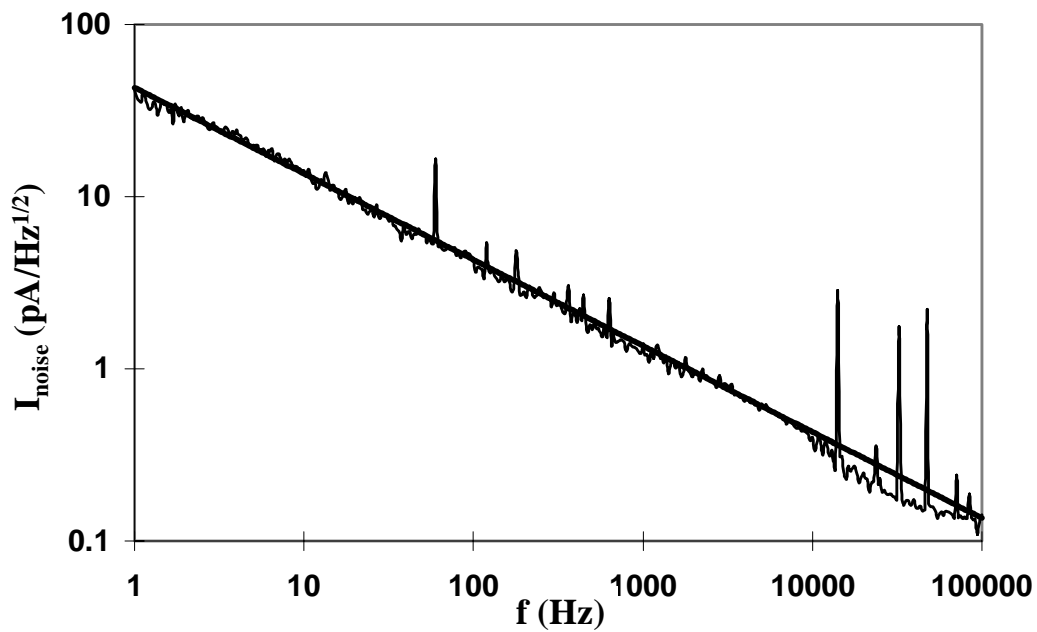


Figure 10. Noise current as a function of frequency at $80K$ for a reverse bias of $200mV$ on a log-log scale. The solid line is of the form $\frac{1}{f^{0.5}}$ indicating that the noise is detector dependent.

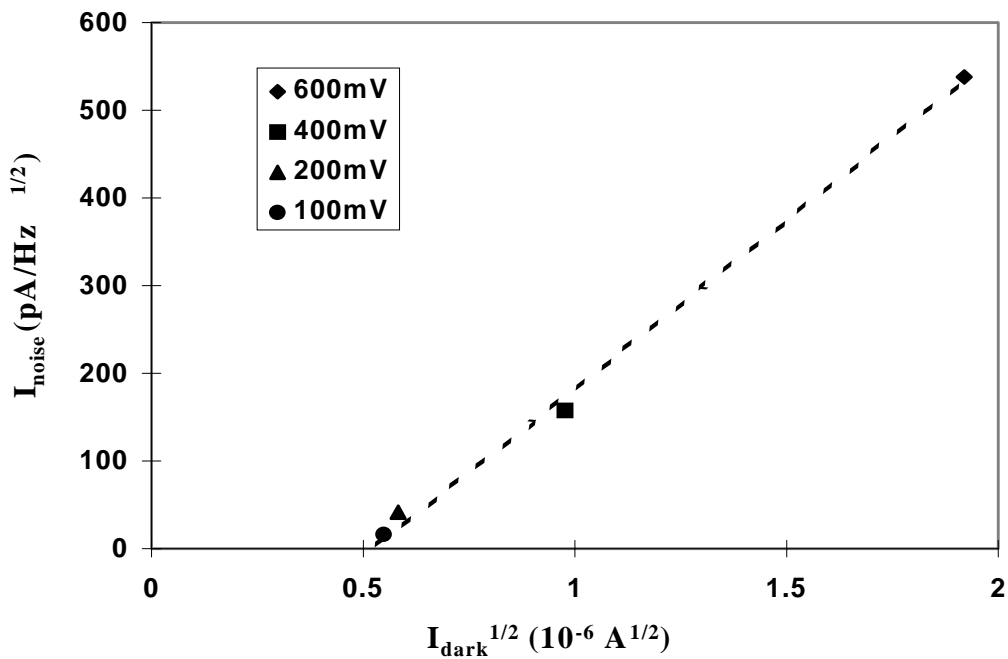


Figure 11. Noise current as a function of the square root of the dark current for the upper junction. The dashed line gives a slope of about 4×10^{-4} .